Atmos. Chem. Phys. Discuss., 15, 29079–29124, 2015
www.atmos-chem-phys-discuss.net/15/29079/2015/
doi:10.5194/acpd-15-29079-2015

Atmospheric Chemistry and Physics Discussions

Processes controlling the seasonal cycle of Arctic aerosol number and size distributions

B. Croft[1], R. V. Martin[1,2], W. R. Leaitch[3], P. Tunved[4], T. J. Breider[5], S. D. D'Andrea[6], and J. R. Pierce[6,1]

[1]Department of Physics and Atmospheric Science, Dalhousie University, Halifax, NS, Canada
[2]Harvard-Smithsonian Center for Astrophysics, Cambridge, MA, USA
[3]Science and Technology Branch, Environment Canada, Toronto, Ontario, Canada
[4]Department of Environmental Science and Analytical Chemistry, Stockholm University, Stockholm, Sweden
[5]School of Engineering and Applied Sciences, Harvard University, Cambridge, MA, USA
[6]Department of Atmospheric Science, Colorado State University, Fort Collins, CO, USA

Received: 2 October 2015 – Accepted: 10 October 2015 – Published: 27 October 2015

Correspondence to: B. Croft (bcarlin@dal.ca)

Published by Copernicus Publications on behalf of the European Geosciences Union.

Abstract

Measurements at high-Arctic sites show a strong seasonal cycle in aerosol number and size. The number of aerosols with diameters larger than 20 nm exhibits a maximum in late spring associated with a dominant accumulation mode (0.1 to 1 µm in diameter), and a second maximum in the summer associated with a dominant Aitken mode (10 to 100 nm in diameter). Seasonal-mean aerosol effective diameter ranges from about 180 nm in summer to 260 nm in winter. This study interprets these seasonal cycles with the GEOS-Chem-TOMAS global aerosol microphysics model. We find improved agreement with in-situ measurements of aerosol size at both Alert, Nunavut, and Mt. Zeppelin, Svalbard following model developments that: (1) increase the efficiency of wet scavenging in the Arctic summer and (2) represent coagulation between interstitial aerosols and aerosols activated to form cloud droplets. Our simulations indicate that the dominant summertime Aitken mode is associated with increased efficiency of wet removal, which limits the number of larger aerosols and promotes local new-particle formation. We also find an important role of interstitial coagulation in clouds in the Arctic, which limits the number of Aitken-mode aerosols in the non-summer seasons when direct wet removal of these aerosols is inefficient. Total aerosol number reaches a minimum in October at both Alert and Mt. Zeppelin. Our simulations indicate that this October minimum can be explained by diminishing local new-particle formation, limited transport of pollution from lower latitudes, and efficient wet removal. We recommend that the key processes of aerosol wet removal, interstitial coagulation and new-particle formation be carefully considered in size-resolved aerosol simulations of the Arctic. Uncertainties about these processes, which strongly control the seasonal cycle of aerosol number and size, limit confidence in estimates of aerosol radiative effects on the Arctic climate.

ACPD
15, 29079–29124, 2015

1 Introduction

The climate impact of aerosols strongly depends on aerosol number, mass, and size distributions (Haywood and Boucher, 2000; Lohmann and Feichter, 2005). These aerosol properties, in addition to chemical composition, contribute to aerosol effects on the Earth's climate. Aerosols influence the global climate directly through scattering and absorption of radiation (Charlson et al., 1992), and indirectly by modifying cloud properties (Twomey, 1974; Albrecht, 1989). Particularly in the Arctic, observations show a strong seasonal cycle in aerosol number and size distributions (Tunved et al., 2013). In this study, we focus on understanding the processes that control Arctic aerosol number and size distributions and their seasonal cycle.

In the high Arctic at Mt. Zeppelin, Svalbard, the observed seasonal cycle in aerosol number exhibits two maxima, one in April, associated with accumulation-mode particles and one in July, associated with smaller, Aitken-mode particles. Tunved et al. (2013) proposed that these seasonal transitions are controlled by changes in aerosol wet removal and source regions since more efficient wet removal in the mid latitudes and within the Arctic in late spring and summer could inhibit transport of aged accumulation-mode aerosols into the Arctic. These summertime conditions favor aerosol formation and growth within the Arctic by reducing the condensation sink for sulfuric acid since there is less aerosol surface area in accumulation mode size range (Leaitch et al., 2013; Heintzenberg et al., 2015). This seasonal transition from springtime accumulation-mode-dominated to summertime Aitken-mode-dominated distributions has been observed not only at surface sites, but also in the free troposphere (Engvall et al., 2008).

Previous studies have used observations and models to examine the role of transport and scavenging in the seasonal cycle of Arctic aerosol mass abundance (Garrett et al., 2010, 2011; Browse et al., 2012; DiPierro et al., 2013; Sharma et al., 2013; Stohl et al., 2013). However, there has been considerably less focus on the seasonal cycle of Arctic aerosol number and size distributions. Few previous studies have used a global

ACPD
15, 29079–29124, 2015

model to interpret the seasonal cycle of in-situ Arctic aerosol number and size observations and the processes that control these seasonal cycles (e.g. Korhonen et al., 2008; Leaitch et al., 2013).

In this study, we examine the seasonal cycle of aerosol size distributions at the Canadian high-Arctic measurement site at Alert, Nunavut (82.5° N) and also include measurements at Mt. Zeppelin, Svalbard (79° N). We use the GEOS-Chem global chemical transport model with the size-resolved aerosol microphysics package TOMAS (D'Andrea et al., 2013; Pierce et al., 2013; Trivitayanurak et al., 2008) to examine the relative importance of various aerosol processes (new-particle formation, emissions, removal and microphysical processes such as condensation and coagulation) in controlling the seasonal cycle of aerosol number and size distributions in the Arctic.

In the following section, we describe the high-Arctic measurements and give an overview of the GEOS-Chem-TOMAS model and the simulations conducted for this study. Section 3 examines the monthly and seasonal mean in-situ observations of aerosol number and size from scanning mobility particle sizer (SMPS) at Alert, and includes comparisons with differential mobility particle sizer (DMPS) measurements at Mt. Zeppelin. The GEOS-Chem-TOMAS model is used to interpret the seasonal cycle of these measurements. We subsequently present the process rates that contribute to the aerosol seasonal cycles in our simulations.

2 Method

2.1 Measurements at Alert

Measurements of particle size distributions at Alert have been ongoing since March 2011 with the exception of a few technical interruptions. Sampling of the ambient aerosol size distribution at Alert was conducted as described by Leaitch et al. (2013). Briefly, the particles are sampled through stainless steel with a mean residence time for a particle from outside to its measurement point of approximately 3 s. At the point

ACPD
15, 29079–29124, 2015

of sampling, the aerosol is at a temperature (T) of approximately 293 K and a relative humidity (RH) is < 50 %. The particle size distributions from 20 to 500 nm diameter are measured with a TSI 3034 Scanning Mobility Particle System (SMPS), operating at a flow rate of 1.0 L min^{-1} and verified for sizing on site using monodisperse particles of polystyrene latex and of ammonium sulfate generated with a Brechtel Manufacturing Incorporated (BMI) Scanning Electrical Mobility Spectrometer (SEMS) and for number concentrations through comparison with a TSI 3772 Condensation Particle Counter (CPC). The Alert SMPS data are accurate to within 15 %, in terms of number concentration and sizing. The total number concentration of particles > 10 nm at Alert is measured with a TSI 3772 CPC operating at a flow rate of 1.0 L min^{-1}. The 3772 CPC was initially compared with a TSI 3776 CPC temporarily operating at the site, and the differences were found to be < 10 % when particle sizes were large enough such that all particles were counted by both counters. The 3772 CPC also compares to within 10 % with SMPS when particle sizes are large enough for all particles to be counted by both instruments (e.g. during periods of Arctic Haze).

Figure A1 shows the seasonal cycle of the Alert SMPS total number concentrations of aerosols with diameters between (1) 20–500 nm (total SMPS), (2) 20–50 nm, (3) 100–500 nm (N100) and (4) 200–500 nm (N200) for the years 2011, 2012 and 2013. A robust seasonal cycle in aerosol number occurs each year at Alert. Total aerosol number reaches a minimum in early fall. There are two maxima, one in spring associated with the accumulation mode size (N100 and N200) and the second in summer associated with smaller Aitken mode particles with sizes in the 20 to 50 nm range. This is similar to the findings of Tunved et al. (2013) for Mt. Zeppelin.

2.2 Measurements at Mt. Zeppelin

The Department of Environmental Science and Analytical Chemistry, Section for Atmospheric research (ACES), Stockholm University (SU), has monitored the sub-micron aerosol number size distribution at Mt. Zeppelin since 2000 with a differential mobility particle sizer (DMPS). Today, this more than 15-year continuous dataset constitutes

ACPD
15, 29079–29124, 2015

one of the longest unbroken aerosol number size distribution observation series in the Arctic. The inlet of the station is a heated whole air inlet.

During the 15 years of operation, the DMPS system has undergone a number of modernizations. Initially a single differential mobility analyzer (DMA) system was used covering a size range between roughly 20–600 nm. A major overhaul was however performed during late 2010, and since then the setup has remained unchanged. The data used in this study thus come from the same instrument configuration.

The current DMPS-system utilizes a custom-built twin DMA setup comprising one Vienna-type medium DMA coupled to a TSI CPC 3772 covering sizes between 25–800 nm and a Vienna-type long DMA coupled with at TSI CPC3 010 effectively covering sizes between 5–60 nm. A Ni-63 neutralizer is used. The size distributions from the two systems are harmonized on a common size grid and then merged. Both systems use a closed-loop setup. RH and T are internally monitored and dry conditions with RH < 30 % typically apply. The system is regularly checked with latex spheres and flow controls. The data are manually screened and crosschecked with other available observations.

2.3 GEOS-Chem-TOMAS model description

In this study, we use the GEOS-Chem-TOMAS model, which couples the GEOS-Chem global chemical transport model (www.geos-chem.org, Bey et al., 2001) with the TwO-Moment Aerosol Sectional (TOMAS) microphysics scheme (Adams and Seinfeld, 2002; Lee and Adams, 2012). All simulations use GEOS-Chem version 9.02 at $4^{\circ} \times 5^{\circ}$ resolution globally, with 47 layers extending from the surface to 0.01 hPa. Assimilated meteorology is from the National Aeronautics and Space Administration (NASA) Global Modelling and Assimilation Office (GMAO) Goddard Earth Observing System version 5 (GEOS-5). All simulations use meteorology and emissions for the year 2011 following 3 months spin-up at the end of 2010. GEOS-Chem includes simulation of more than 50 gas-phase species including oxidants such as OH and aerosol precursor gases such as SO_2 and NH_3. Emissions in GEOS-Chem-TOMAS are described in detail in

ACPD
15, 29079–29124, 2015

Stevens and Pierce (2014). In addition, we implement seabird colony NH_3 emissions from Riddick et al. (2012) with modifications for additional colonies in the Arctic region based on the on-line Circumpolar Seabird Data Portal (Seabird Information Network, 2015) as described and evaluated in Wentworth et al. (2015) and Croft et al. (2015). We include both biogenic ($\sim 19\,Tg\,yr^{-1}$) and anthropogenically enhanced ($100\,Tg\,yr^{-1}$, spatially correlated with anthropogenic CO emissions) secondary organic aerosol (SOA) and consider this SOA non-volatile following D'Andrea et al. (2013). The TOMAS microphysics scheme tracks the number and mass of particles within each of 15 size sections. The first 13 size sections are logarithmically spaced, and include aerosol diameters from approximately 3 nm to 1 µm, and 2 additional size sections represent aerosol diameters from 1 to 10 µm (Lee and Adams, 2012). Simulated species are sulfate, ammonia, sea-spray, hydrophilic organics, hydrophobic organics, internally mixed black carbon, externally mixed black carbon, dust and water. Aerosol hygroscopic growth is a function of grid box mean relative humidity capped at 99 %. For these simulations, new-particle formation is treated according to the state-of-the-art ternary H_2SO_4-NH_3-H_2O nucleation scheme described by Baranizadeh et al. (2015). The formation rate of particles at circa 1.2 nm in mass diameter is determined from a full kinetics simulation by Atmospheric Cluster Dynamics Code (ACDC; Olenius et al., 2013) using particle evaporation rates based on quantum chemistry. The scheme is implemented as a comprehensive look-up table of simulated formation rates as a function of sulfuric acid and ammonia vapor concentrations, relative humidity, temperature, and condensation sink. Growth and loss of particles with diameters smaller than 3 nm are approximated with the Kerminen et al. (2004) scheme (evaluated in TOMAS in Y. H. Lee et al., 2013).

In our simulations, aerosols are removed from the atmosphere by precipitation both in and below clouds, and also by dry deposition (Liu et al., 2001). The in-cloud wet scavenging parameterization in the standard GEOS-Chem-TOMAS module uses the same equations for the removal efficiency and the precipitation fraction as in the bulk-aerosol GEOS-Chem module described in Liu et al. (2001) with updates implemented by Wang et al. (2011) to account for wet removal in mixed-phase and ice clouds. How-

ACPD
15, 29079–29124, 2015

ever, the aerosol in-cloud wet removal in GEOS-Chem-TOMAS is limited to the aerosol size range that is assumed to be activated into cloud hydrometeors.

2.4 Simulations and revisions to model parameterizations

Table 1 summarizes the four simulations conducted with the GEOS-Chem-TOMAS model. These simulations include (1) a standard, (2) updates to wet removal, (3) interstitial coagulation of aerosols in clouds, and (4) a sensitivity test related to new-particle formation. The first (simulation STD) uses the standard GEOS-Chem-TOMAS model as described above.

Simulation NEWSCAV introduces developments to the wet removal parameterization to allow for variable in-cloud water content, to implement a temperature-dependent aerosol activation fraction, and to more closely relate in-cloud aerosol scavenging to cloud fraction. The standard GEOS-Chem-TOMAS wet removal efficiency β for large-scale clouds is based on a parameterization originally developed by Giorgi and Chameides (1986):

$$\beta = k_{\min} + Q/L \quad (1)$$

where Q is the grid-box mean precipitation production rate [$\mathrm{g\,cm^{-3}\,s^{-1}}$] from the GEOS-5 meteorological fields, L is the in-cloud liquid and ice water content [$\mathrm{g\,cm^{-3}}$] of the precipitating clouds (an assumed constant) and $k_{\min}$ is a constant, $1 \times 10^{-4}\,\mathrm{s^{-1}}$. The $k_{\min}$ term represents autoconversion processes that produce precipitation. The Q/L term represents accretion processes. The standard GEOS-Chem model uses a globally fixed value for L of $1 \times 10^{-6}\,\mathrm{g\,cm^{-3}}$. While this value has been found to perform well for wet scavenging in a global sense (Liu et al., 2001; Wang et al., 2011), the value does not well represent observations in certain regions. Measurements by Shupe et al. (2001) and Leaitch et al. (2015) show an Arctic spring-summer-mean cloud liquid water content that is an order of magnitude lower ($1 \times 10^{-7}\,\mathrm{g\,cm^{-3}}$). During the spring and summer, more efficient aerosol removal in liquid clouds plays a key role in the

ACPD
15, 29079–29124, 2015

control of aerosol distributions (Garrett et al., 2010). An overestimation of the liquid water content of Arctic clouds (by using a globally fixed value for L) in our simulation would yield an under-vigorous wet removal efficiency, particularly for cases of low intensity precipitation (low Q). To address this issue, we replace the fixed value with the cloud liquid and ice water contents from the GEOS-5 assimilated meteorology fields and calculate the efficiency as the ratio of the grid-mean precipitation production rate and the grid-mean liquid and ice water contents. We impose a maximum efficiency of 1×10^{-3} s^{-1} to prevent over-vigorous removal.

In addition, we implement a temperature-dependent representation of the aerosol activated fraction (Verheggen et al., 2007) to account for the fraction of aerosol susceptible to wet removal in mixed-phase clouds. In mixed-phase clouds, only a fraction of the aerosols are contained in the cloud hydrometeors and susceptible to removal when cloud water and ice converts to precipitation. As clouds glaciate, cloud droplets evaporate and release aerosols from the condensed phase because ice crystals grow at the expense of cloud droplets due to differences in the saturation vapour pressure over liquid water and ice. The Verheggen et al. (2007) parameterization for activated fraction accounts for this effect, such that only a fraction of the total in-cloud aerosol is susceptible to wet removal as precipitation forms in mixed phase clouds. However, in strongly riming-dominated regimes, this may lead to an under-estimate of the removal.

We also develop the representation of the precipitation fraction. In the standard GEOS-Chem model, the fraction of the grid box that is precipitating, F, is

$$F = Q/L \tag{2}$$

Replacing β with Eq. (1) and simplifying yields

$$F = 1/(1 + (k_{\min} \cdot L/Q)) \tag{3}$$

where $k_{\min} \cdot L$ has a fixed value of 1×10^{-10} g cm^{-3} s^{-1} in the standard model version. Thus, the precipitation fraction increases with precipitation production rate. We replace this parameterization by treating the precipitation fraction for aerosol scavenging in

ACPD
15, 29079–29124, 2015

clouds as the cloud fraction from the GEOS-5 meteorological fields in the model layers where precipitation is produced. These wet scavenging developments were also implemented in a GEOS-Chem v9-03-01 simulation of ^{137}Cs (also using GEOS5 met fields) and evaluated against ^{137}Cs measurements taken for several weeks following the March 2011 Fukushima Dai-Ichi nuclear power plant accident. Implementation of these scavenging revisions yielded improved agreement with the radionuclide measurements (median ratio of measurement to modeled surface layer concentrations changed from 5.53 to 0.52) and reduced e-folding times from 21.8 to 13.2 days, which is close to the measurement value of 14.3 days (Kristiansen et al., 2015). These wet removal revisions also slightly reduced the mean bias relative to measurements of the number of aerosols larger than 40 nm (N40), 80 nm (N80) and 150 nm (N150) for the same global set of 21 geographically diverse sites as described in Pierce et al. (2014) (not shown). Future work will include further global evaluation of the GEOS-Chem wet removal scheme.

Simulation NEWSCAV + COAG includes additional developments to the interstitial aerosol coagulation mechanism in clouds for the TOMAS microphysics scheme as explored in detail in Pierce et al. (2015). This revised coagulation parameterization accounts for the order 100-fold increase in the wet size of aerosols that activate to form cloud droplets. This simulation assumes that (1) aerosols that activate to form cloud droplets must have a dry diameter larger than 80 nm, (2) super-cooled clouds persist to temperatures as low as 238 K and (3) all cloud droplets are 10 µm in diameter. While these are crude assumptions, they are within reasonable bounds and allow examination of the potential of interstitial coagulation to control aerosol size distributions. The grid-box mean coagulation kernel between two size bins is calculated as

$$J_{i,j} = (1 - f_{\text{cloudy}})K_{\text{clear};i,j}N_iN_j + f_{\text{cloudy}}K_{\text{cloudy};i,j}N_iN_j \quad (4)$$

where $J_{i,j}$ is the coagulation rate between particles in bins i and j, f_{cloudy} is the fraction of the grid box that is cloudy, K_{clear} is the coagulation kernel between bins i and j in the clear portion of the gridbox, K_{cloudy} is the coagulation kernel between bins i and j

ACPD
15, 29079–29124, 2015

in the cloudy portion of the gridbox, N_i is the number concentration of particles in bin i, and N_j is the number concentration of particles in bin j. While the activated particle is assumed to have a diameter of 10 µm, the unactivated collision-partner aerosol is assumed to have a diameter following hygroscopic growth under grid-box mean relative humidity. If the in-cloud relative humidity is considerably greater than the grid mean, then the coagulation kernel could be overestimated. These developments to the interstitial aerosol coagulation parameterization in clouds are applied and evaluated in Pierce et al. (2015) and yield improved agreement with in-situ aerosol size distributions at 21 geographically diverse sites in the Northern Hemisphere.

Simulation NONUC turns off all new particle formation (NPF) to examine the contribution of NPF to aerosol number in the Arctic. This simulation is otherwise identical to simulation NEWSCAV.

3 Observations and GEOS-Chem-TOMAS simulations of seasonal cycles in Arctic aerosol number and size

3.1 Observed seasonal cycle of aerosol number distribution in the Arctic

Figure 1 shows the 2011–2013 monthly mean aerosol number distributions from the SMPS at Alert and DMPS at Mt. Zeppelin. At both sites, the accumulation mode (defined here as 0.1 to 1 µm in diameter) gradually builds during winter to a maximum in March and April. Afterward, the accumulation mode decreases while the Aitken mode (0.01 to 0.1 µm in diameter) increases in number to a maximum in July–August. The early autumn months are characterized by the lowest number concentrations in both modes until the accumulation mode starts to build again in November. This seasonal cycle is remarkably similar at both sites and similar to that observed at Mt. Zeppelin over a ten year period from 2000 to 2010 (e.g. Fig. 7 in Tunved et al., 2013). The similarity in these number distributions across the 1000 km that separates Alert and Mt. Zeppelin suggests a cycle that spans the high Arctic. In the following sections we

ACPD
15, 29079–29124, 2015

use the GEOS-Chem-TOMAS model to interpret the processes that control these cycles.

Figure 2 shows the median total particle number concentrations [cm^{-3}] from measurements made with the SMPS at Alert and DMPS at Mt. Zeppelin. Again, both high-Arctic sites exhibit a similar seasonal cycle despite their geographic separation. The total aerosol number has a shallow maximum in the spring and summer at both locations. The magnitude between the 20th to 80th percentiles is greatest during the months of April to September when local new-particle formation processes are expected to contribute episodically to the total aerosol number. We examine this further in Sect. 3.3.

Figure 3 shows the aerosol effective diameter calculated from measurements with the SMPS at Alert (2011–2013) and the DMPS at Mt. Zeppelin (2011–2013). The effective diameter is the ratio of the second and third moments of the aerosol number distribution and is useful in determining the optical properties of an aerosol distribution, and for comparing between distributions. The effective diameter is defined as

$$D_{\text{eff}} = \int_{D_{\min}}^{D_{\max}} D^3 N(D) \mathrm{d}D \Big/ \int_{D_{\min}}^{D_{D_{\max}}} D^2 N(D) \mathrm{d}D \tag{5}$$

where D is the aerosol diameter and $N(D)$ is the aerosol number distribution. The integral here is taken over the size range from $D_{\min} = 20\,\text{nm}$ to $D_{\max} = 500\,\text{nm}$. Despite the geographic distance of these two sites, the seasonal cycle of the aerosol effective diameter is remarkably similar. At both sites, the aerosol effective diameter shows a strong seasonal cycle with a minimum during the summer months of about 180 nm and a maximum in the winter of about 260 nm. The effective diameter at Mt. Zeppelin exceeds Alert by about 10–20 % throughout the year. This may indicate a greater abundance of precursor material for aerosol growth at Mt. Zeppelin, but could also be related to differences in instrument calibration at the two sites. In the next sections, we interpret

ACPD
15, 29079–29124, 2015

these observed seasonal cycles in number and size using the GEOS-Chem-TOMAS model.

3.2 Evaluation of GEOS-Chem-TOMAS simulations with in-situ measurements

Figures 4 and 5 show the seasonal-median number distributions measured at Alert and Mt. Zeppelin, respectively and also the simulated number distributions for our four simulations. The measurements show a dominant Aitken mode in summer, whereas other seasons have a dominant accumulation mode. The measurement values exhibit the greatest variability in summer, a feature that has been associated with shorter aerosol lifetimes (William et al., 2002; Tunved et al., 2004). We investigate aerosol lifetime further in Sect. 3.3. For both sites, the standard simulation (STD on Figs. 4 and 5) overestimates the number of accumulation-mode aerosols (diameters 100–500 nm) in all seasons. Revisions to the wet scavenging parameterization (simulation NEWSCAV) reduce the accumulation mode in summer when scavenging of this size range is of highest efficiency and is expected to strongly control aerosol number in this size range. The factor of two reduction in the number of accumulation mode aerosols in the summer yields very close agreement (within 20 %) with the observations. Breider et al. (2015) evaluated a similar revised scavenging parameterization in a mass-based GEOS-Chem aerosol simulation and found a similar effect that improved agreement with summertime Arctic in-situ sulfate mass concentrations. In other seasons, wet scavenging has less control on accumulation mode number, and revisions to wet scavenging have less effect in non-summer seasons.

Figures 4 and 5 also show that the simulations STD and NEWSCAV over-predict the number of Aitken-mode aerosols (diameters 10–100 nm) in the non-summer seasons. Indeed, the overprediction worsens for NEWSCAV since the more vigourous scavenging reduces the condensation sink and favors new-particle formation, yielding more Aitken mode aerosols globally. Simulation NEWSCAV + COAG demonstrates that the prediction of the number of Aitken mode aerosols in the non-summer seasons is highly sensitive to the parameterization of interstitial aerosol coagulation in clouds.

ACPD
15, 29079–29124, 2015

The number of Aitken and smaller accumulation mode aerosols is reduced by the implementation of this process. As discussed in Pierce et al. (2015), the reduction of Aitken-mode particles occurs due to coagulation scavenging by aerosols that activated to form clouds drops, and the reduction in accumulation-mode particles occurs because fewer Aitken-mode particles are available to grow to accumulation-mode sizes. Pierce et al. (2015) quantify the potential influence of this process on the global aerosol direct and indirect effects on the global radiation budget. Among our four simulations, the NEWSCAV + COAG simulation gives the closest representation of the number of non-summer Aitken and accumulation mode aerosols relative to the in-situ measurements at both Alert and Mt. Zeppelin. Simulation NEWSCAV + COAG provides a correction of the Aitken mode overestimation in the non-summer seasons in the STD and NEWSCAV simulations. Cesana et al. (2012) analyzed CALIOP retrievals using the cloud phase detection algorithm and found that low-level liquid clouds are ubiquitous in all seasons in the Arctic. Thus, while our assumptions about the presence of liquid clouds at temperatures above 238 K can be viewed as a sensitivity simulation, the assumption is reasonable.

Figures 4 and 5 show that in summer, the simulations NEWSCAV and NEWSCAV + COAG capture the dominant Aitken mode. This is due to increased new-particle formation in the Arctic that occurs in response to a lower condensation sink (less aerosol surface area in the accumulation mode) during the summertime coupled with a greater availability of sulfuric acid from the oxidation of locally formed precursor gases such as dimethyl sulfide (DMS) (Leaitch et al., 2013). However, the simulation at Alert overestimates the number of aerosols with diameters smaller than 30 nm. At both Alert and Zeppelin, our simulations underestimate the summertime number of larger Aitken mode aerosols (50–100 nm). This may be the result of not enough material to contribute to new-particle growth in the simulation. Another possibility is an excessive number of new particles competing for condensable material for growth and suppressing growth overall into the 50–100 nm size range. However, at Zeppelin the number of 20–30 nm aerosols is reasonably well simulated and yet the upper-Aitken-range underestimation

ACPD
15, 29079–29124, 2015

persists. This under-prediction of the number 50–100 nm particles also persisted in a sensitivity test using a scaled Napari nucleation scheme as in Westervelt et al. (2013), combined with the binary ($H_2SO_4 + H_2O$) nucleation scheme of Vehkamäki et al. (2002) in the regions with low NH_3 (not shown). Although the over prediction of the number of 20–30 nm at Alert was reduced. As well, we tested the implementation of condensation of methanesulfonic acid (MSA) to contribute to new particle growth. However, this was insufficient. Our neglect of primary organic emissions from the oceans or volatile organic compounds that could contribute to growth could play a role (O'Dowd and de Leeuw, 2007; Fu et al., 2013) and will be examined in future studies.

Of the four simulations, NEWSCAV + COAG provides the closest agreement with the measurements at both sites and for all seasons, highlighting the importance of the wet removal and interstitial coagulation processes. In the following paragraphs, we further evaluate these simulations by considering integration over the simulated and observed size distributions. Figures 4 and 5 also indicate that simulation NEWSCAV + COAG captures the general pattern of a dominant Aitken mode in summer and a dominant accumulation mode in the other seasons at both Alert and Mt. Zeppelin, a key feature that was missing in simulation STD. Croft et al. (2015) find that new particle formation (NPF) is strongly sensitive to the representation of the NH_3 from Arctic seabird emissions. As a result, error in the prediction of summertime particle number between diameters of 20 and 80 nm may reflect errors in the exact strength of this NH_3 source, and its interseasonal and interannual variation at both the Alert and Mt. Zeppelin sites.

Figures 4 and 5 also show the results from a simulation NONUC based on simulation NEWSCAV but with all aerosol nucleation turned off. This unphysical simulation still overestimates the number of Aitken mode aerosols at Alert and Mt. Zeppelin in the fall and winter. Thus, errors in the new-particle formation processes cannot account for the non-summer Aitken mode overprediction, supporting our findings that interstitial coagulation in clouds is an important control of the non-summer Aitken mode. However, there remains the possibility that errors in primary emissions could also contribute to this Aitken mode overprediction. Simulation NONUC also demonstrates that NPF

ACPD
15, 29079–29124, 2015

largely controls the total number of aerosols in the summer when more than 75 % of the total number of aerosols is attributed to NPF.

Figures 6 and 7 show the seasonal cycle of the median number of particles with diameters between 20–500 nm (N20), 80–500 nm (N80), and 200–500 nm (N200) from measurements with the SMPS at Alert and the DMPS at Mt. Zeppelin. A measurement limit of 20–500 nm is applied to the Mt. Zeppelin data to be consistent with the Alert data. The simulated N20, N80 and N200 are also shown for our four simulations with upper size limit of 500 nm applied to be consistent with the measurements. The summertime minimum in N200 is over-predicted by about a factor of two for simulation STD. Wet removal revisions for simulation NEWSCAV yield a factor of two reduction to give very close (within 20 %) agreement with the measurements. Among our four simulations, the simulation NEWSCAV + COAG yields the closest agreement with the integrated number measurements (N20, N80, N200) in all seasons at both sites. Implementation of interstitial coagulation in clouds in simulation NEWSCAV + COAG achieves a twofold reduction in N20 during the winter months that reduces the bias in simulations STD and NEWSCAV. The 3-fold wintertime over-prediction of N20, N80 and N200 at Mt. Zeppelin could be related to an over-prediction of the wintertime emissions in regions outside the Arctic. The summertime N20 is under-predicted at Mt. Zeppelin but over-predicted in July at Alert. Errors related to sources of aerosol precursor gases and neglect of marine organic emissions could contribute to these discrepancies.

Figures 6 and 7 also show the seasonal cycle of effective diameter at Alert and Mt. Zeppelin. The simulation NEWSCAV + COAG has the closest agreement with the seasonal cycle in the measurements. The simulations tend to over-predict the aerosol effective diameter in summer. Missing oceanic sources of small primary organic particles or under-estimation of the source strength of nucleation/growth precursor gases, such as MSA and organics, which could yield more particles with diameters smaller than 100 nm could address this problem and are a subject of ongoing investigation. The over-prediction of summertime effective diameter is pronounced for the simulation NONUC that removes NPF, indicating its importance for the smaller aerosols. Simu-

ACPD
15, 29079–29124, 2015

lation STD also over-predicts the summertime effective diameter by about a factor of two, attributed to under-vigorous scavenging, which yields too many larger particles.

Figure 8 shows the seasonal-mean pan-Arctic geographic distribution of the surface layer effective diameter for the NEWSCAV + COAG simulation. The similarity in the seasonal cycle of effective diameter at Alert and Zeppelin (both simulated and observed) suggests a cycle that occurs throughout the Arctic. Simulation NEWSCAV + COAG exhibits this pan-Arctic cycle, such that the maximum effective diameter is in the winter when the size distribution is dominated by aged accumulation mode aerosol. The pan-Arctic effective diameter declines to a minimum in summer, when local new-particle formation builds a dominant Aitken mode. Overall, revisions to both the wet removal and the interstitial coagulation parameterizations yield an encouraging improvement in our simulation in comparison with in-situ measurements at both the Alert and Mt. Zeppelin. In the following section, we use simulation NEWSCAV + COAG to examine the relative contributions of emissions, transport, microphysics and removal to the seasonal cycle of number and size in the Arctic.

3.3 Process rates controlling the seasonal cycle in Arctic aerosol number and size

Figure 9 shows the seasonal cycle of regional-mean process rates that control aerosol number for the entire Arctic troposphere north of the Arctic circle (north of 66° N) for the simulation NEWSCAV + COAG. Each of four aerosol size ranges is considered separately. Source processes are positive and sink processes are negative. The number of nucleation mode aerosols is controlled primarily by the nucleation source and coagulation sink processes. There are two maxima in the nucleation rate, one in early spring when precursors are abundant, and one in summer when there is a low condensation sink and greatest local precursor emissions. These rates are derived by an integration over the entire troposphere to obtain budget closure. As a result, the early spring maxima, which is associated nucleation at high altitudes in our simulations, is not evident in the in-situ measurements. During winter, transport reaches a seasonal maximum and

ACPD
15, 29079–29124, 2015

nucleation (new-particle formation) reaches a seasonal minimum such that the two are comparable sources of nucleation mode aerosols to the Arctic.

Figure 10 shows the regional-mean transport across the Arctic circle boundary as a function of altitude. Nucleation-mode size particles are transported in the mid to upper troposphere (at altitudes between 4 and 10 km) where the coagulation sink is sufficiently low that nucleation mode particles can persist and be transported into the Arctic. These transport rates are greatest from December to April.

Figure 9 also indicates that several processes control the Aitken mode in our simulation. Northward transport is the dominant source process for the Arctic Aitken mode, accounting for more than 75 % of the total source rate during all months of the year. This transport of Aitken-mode aerosols occurs at all vertical levels below 10 km as shown in Fig. 10. Figure 9 shows that during the Arctic spring, when the total aerosol mass is greatest, condensation on existing aerosols makes a relatively greater contribution (about 20 %) to the total source rates for Aitken mode particles. This net enhancement is compensated by the rate of condensational growth as a loss of Aitken-mode particles to accumulation-mode sizes such that the nucleation mode is a larger source of Aitken-mode particles than shown here. Primary particle emissions within the Arctic account for about 10–20 % of the source rate throughout the year in our simulation. Coagulation is the dominant sink for the Aitken mode with dry deposition accounting for about 20–25 % of remaining sink. Removal by wet deposition is weak as the smaller Aitken mode aerosols are not large enough to be susceptible to the efficient removal by activation scavenging (the process of aerosols acting as the seed for cloud-droplet and ice-crystal formation and subsequent conversion to rain or snow during precipitation formation) in our simulation. However, recent studies indicate that aerosols as small as 50–60 nm can activate in the clean Arctic summertime conditions (Leaitch et al., 2013, 2015) and we likely under-estimate this removal in our simulations.

For the accumulation mode, Fig. 9 indicates that in our simulation the dominant sources for aerosol number are northward transport and condensation, which also includes sulfate production by in-cloud oxidation. These two source terms are roughly

ACPD
15, 29079–29124, 2015

equal in magnitude in the Arctic throughout the year in our simulations. Northward transport of accumulation-mode aerosols persists at a similar magnitude in the simulation in all seasons, with a shallow minimum in winter. Figure 10 shows that transport in the mid troposphere (altitudes 4 to 10 km) reaches a maximum in March–April, which would contribute to the well-known Arctic haze phenomena. Figure 10 also shows that the majority of accumulation mode number transport is below 1.5 km. This persistent low-level transport throughout the summer suggests that the summertime cleanliness of the Arctic near-surface atmosphere relies heavily on the increased efficiency of the removal processes in the lower troposphere during the summer months. Indeed, Fig. 9 shows that wet removal is the dominant sink process in all seasons, but increases in magnitude and relative importance with respect to dry deposition in the summer, accounting for more than 90 % of the total summertime sink rate. In winter, the relative importance of dry deposition increases, although remains below 25 % of the total sink rate in our simulation.

Figure 9 indicates that the coarse mode in our simulation is controlled primarily by emissions, transport and wet deposition. In the late spring, northward transport of dust combined with local sea-salt emissions is not quite matched by the removal processes in the simulation. The inverse of the resultant residual (black line on Fig. 9) gives the net rate of either aerosol build-up (accumulation) or loss for the regional monthly mean number. In early spring, there is a net build-up of coarse mode aerosol in the Arctic region. However as spring progresses, there is a net loss such that the net residual (net accumulation or loss rate) integrates to zero over the annual cycle. Wet removal is the primary loss process in all seasons in this simulation. Figure 10 shows that the early spring-time transport occurs mainly at altitudes above 4 km, a time when the polar dome still extends relatively far southward.

We noted in the discussion of Fig. 1 that the total aerosol number reaches a minimum at both Alert and Mt. Zeppelin in October. The processes shown in Fig. 9 explain this October minimum. As the sun sets in the Arctic, new-particle formation (nucleation), condensation, and also northward transport rates approach their minimum, while wet

ACPD
15, 29079–29124, 2015

removal remains relatively efficient. The combined effect contributes to a minimum in total aerosol number in October.

Figures A2, A3 and A4 place the relative importance of these processes controlling the Arctic seasonal cycle in context with the processes controlling the budgets in the regions of the entire troposphere (1) north of 50° N, (2) in the high Arctic (north of 78° N), and (3) globally. The importance of transport decreases for regions with progressively larger southerly extent. The relative increase in wet removal rates in the summer decreases outside the Arctic. In the global budget, wet removal is the dominant sink process for the accumulation and coarse modes (about 80 % of the net sink rate), while coagulation is the dominant sink for the Aitken and nucleation modes, with dry deposition accounting for about 40 % of the Aitken mode number sink. Thus, these number budgets exhibit a strong dependence on latitude. Although our calculations include the changes in regional volume of the troposphere that occur from month to month due to fluctuations in temperature at tropopause height, this introduces less than 10 % change in the magnitude of the rates presented here.

In our discussion of Figs. 9 and 10, we remarked on the importance of seasonal, latitudinal and altitude-dependent changes in wet deposition in the Arctic. Figure 11 shows the simulated lifetime of aerosol number with respect to wet deposition in the troposphere considering layers between 0–1.5, 1.5–4 and 4–10 km and for the regions north of 50, 66 and 78° N and also for the global mean. These lifetimes may be considered as the inverse of the wet removal efficiency. Figure 11 indicates that the magnitude of this lifetime increases markedly with altitude. This simulated aerosol lifetime with respect to wet removal has a summertime minimum in the Arctic for aerosols in the Aitken, accumulation and coarse size ranges throughout the troposphere. Particularly, the accumulation-mode aerosol lifetime with respect to wet removal at the altitudes of springtime haze (1.5–4 km) decreases from 80 days in March to 5 days in summer. In the boundary layer, the simulated lifetime change for the accumulation-size aerosols is not as great (10 days in winter to 5 days in summer) as the changes found at 1.5–4 km. These 2–10-fold shifts in wet removal efficiency below 4 km strongly contribute to the

ACPD
15, 29079–29124, 2015

cleanliness of the summer Arctic since the majority of the accumulation-size aerosol resides at these altitudes. Figure 11 also shows that similar seasonal cycles occur in our simulations for the entire region of the troposphere north of 50° N and 78° N, but no seasonal cycle is evident in the global mean. For all aerosol sizes, the simulated number lifetimes in the Arctic are generally larger than the global mean at all altitudes and seasons, reflecting the lower efficiency of wet removal in mixed-phase and ice clouds.

4 Conclusions

In this study, we interpreted the seasonal cycle of aerosol number and size in the high Arctic measured from 2011–2013 by SMPS at Alert from 2011 to 2013, and by DMPS at Mt. Zeppelin. The seasonal cycle of effective diameter was remarkably similar at these sites despite their geographic separation of at least 1000 km. The effective diameter had an inter-seasonal range between 180 and 260 nm, with a minimum in the summer. Our simulations indicate that this cycle occurs not only at Alert and Mt. Zeppelin, but throughout the Arctic. We found that at Alert and at Mt. Zeppelin, the summertime aerosol number distribution was dominated by the Aitken mode, whereas the non-summer seasons had a dominant accumulation mode. At both Alert and Mt. Zeppelin there were two maxima in the total number of aerosols in the 20 to 500 nm size range (one in April and one in summer) similar to the seasonal cycle at Mt. Zeppelin presented by Tunved et al. (2013) based on data from 2000 to 2010.

We interpreted these seasonal cycles in aerosol number and size with the GEOS-Chem-TOMAS model. Revisions to increase the efficiency of wet removal in the model were needed to represent the number of accumulation mode aerosols in the summertime. In particular, the globally fixed value for the in-cloud liquid and ice water content of the precipitating clouds (1×10^{-6} g cm^{-3}) used in the standard GEOS-Chem model was replaced by the variable cloud liquid water contents from the GEOS-5 met fields to give a more physical representation of the Arctic cloud liquid and ice water contents, which are generally about one order of magnitude less than the globally fixed value (Shupe

ACPD
15, 29079–29124, 2015

et al., 2001; Leaitch et al., 2015). This change increased the efficiency of wet removal and yielded closer agreement with the summertime measurement of the number of accumulation mode aerosols at both Alert and Mt. Zeppelin. We also implemented the Verheggen et al. (2007) temperature-dependent aerosol activated fraction to account for the fraction of aerosol assumed to be in the cloud droplets and ice crystals for the purposes of wet removal. A similar revision to the bulk GEOS-Chem model wet removal scheme implemented by Breider et al. (2015) also yielded improved agreement with in-situ sulfate mass concentration measurements at Arctic sites.

We added to the GEOS-Chem-TOMAS model a parameterization of the coagulation of interstitial aerosols with aerosols of activated size in clouds. Interstitial coagulation in Arctic clouds reduced the number of Aitken mode aerosols in the non-summer seasons to more closely represent measurements at both Alert and Mt. Zeppelin. In the absence of an interstitial coagulation parameterization, the number of Aitken mode aerosols was over-predicted even in the absence of any new particle formation in the model. Although there exists the possibility of errors in primary emissions and interstitial particle size assuming grid-mean relative humidity, this high sensitivity of aerosol number to interstitial coagulation in clouds suggests that size-resolved models should include this process. However, many present-day global models neglect this process, including previous versions of GEOS-Chem-TOMAS (D'Andrea et al., 2013; Pierce et al., 2013; Trivitayanurak et al., 2008), GISS-TOMAS (Adams and Seinfeld, 2002; Pierce and Adams, 2009), GLOMAP (Spracklen et al., 2005a, b; 2008; Mann et al., 2012), GLOMAP-Mode (Mann et al., 2010, 2012; L. A. Lee et al., 2013), GEOS-Chem-APM (Yu and Luo, 2009; Yu, 2011) and IMPACT (Herzog et al., 2004; Wang and Penner, 2009). To our knowledge, only a few models such as MIRAGE and ECHAM-HAM (Herzog et al., 2004; Ghan et al., 2006; Hoose et al., 2008) represent this process. In our study, we were encouraged to find that our GEOS-Chem-TOMAS simulations yielded close agreement with measurements at Alert and Mt. Zeppelin of the number of aerosols with diameters 20–500 nm (N20), 80–500 nm (N80) and 200–500 nm (N200), as well as with the

ACPD
15, 29079–29124, 2015

aerosol effective diameter and size-resolved number distribution, after revisions to the wet scavenging and with the implementation of an interstitial coagulation scheme.

Simulated process rates indicated that increased wet removal efficiency in summer reduced the number of accumulation mode aerosols, despite ongoing transport of these aerosols into the Arctic during the summer months in our simulations. This wet removal efficiency change from springtime to summertime was about 10-fold at altitudes between 1.5–4 km, which are the altitudes associated with the springtime haze phenomena. This was associated with increased new particle formation rates in summer. New particle formation contributed to the majority of the simulated total summertime aerosol number at the high Arctic sites of Alert and Mt. Zeppelin, based comparisons with a sensitivity simulation without new-particle formation. Reduced wet removal efficiency in the non-summer months allowed greater long-range transport of aerosols in the high Arctic and growth of the accumulation mode to a late spring peak in the model. Interstitial coagulation in the clouds was important in all seasons, and particularly limited the Aitken mode number, except in summer. Total aerosol number reached a minimum in October at both sites, associated with reduced new-particle formation and condensational growth as the sun sets, relatively low northward transport and persistence of relatively high wet removal rates.

The process budgets that control aerosol number could change in a future warming Arctic climate and as emissions within the Arctic change. For example a warmer Arctic could experience more efficient wet removal throughout a greater portion of the year. Emissions in a warmer Arctic may also increase due to increased biological and anthropogenic activity. Changes to these budgets in a future climate should be the subject of future research.

Our results highlight the importance of aerosol processes that continue to be poorly understood, (1) wet removal, (2) new-particle formation, and (3) in-cloud interstitial coagulation, as playing a key role in the control of the seasonal cycle of aerosol number and size in the high Arctic. We recommend that attention be paid to these processes

ACPD
15, 29079–29124, 2015

in size-resolved aerosol simulations of the Arctic and emphasize the ongoing need for work to further knowledge about these processes.

Acknowledgements. The authors acknowledge the financial support provided for NETCARE through the Climate Change and Atmospheric Research Program at NSERC Canada. Thanks to Sangeeta Sharma, Desiree Toom, Andrew Platt and the Alert operators for supporting the Alert observations. We are also grateful to Ilona Riipinen, Jan Julin and Tinya Olenius for helpful discussions and for providing the Atmospheric Cluster Dynamics Code (ACDC), applied in our GEOS-Chem-TOMAS simulations.

References

Adams, P. J. and Seinfeld, J. H.: Predicting global aerosol size distributions in general circulation models, J. Geophys. Res., 107, 4310–4370, 2002.

Adams, P. J. and Seinfeld, J. H.: Disproportionate impact of particulate emissions on global cloud condensation nuclei concentrations, Geophys. Res. Lett., 30, 1210–1239, 2003.

Albrecht, B. A.: Aerosols, cloud microphysics, and fractional cloudiness, Science, 245, 1227–1230, 1989.

Baranizadeh, E., Murphy, B. N., Julin, J., Falahat, S., Fountoukis, C., Reddington, C., Virtanen, A., Pandis, S. N., Vehkamäki, H., Lehtinen, K. E. J., and Riipinen I.: Implementation of state-of-the-art ternary new particle formation scheme to the regional chemical transport model PMCAMx-UF in Europe, in preparation, 2015.

Bey, I., Jacob, D. J., Yantosca, R. M., Logan, J. A., Field, B. D., Fiore, A. M., Li, Q., Liu, H. Y., Mickley, L. J., and Schultz, M. G.: Global modeling of tropospheric chemistry with assimilated meteorology: model description and evaluation, J. Geophys. Res., 106, 23073, doi:10.1029/2001JD000807, 2001.

Breider, T. J., Mickley, L. J., Jacob, D. J., Ge, C., Wang, J., Payer, M., Wang, Q., Fisher, J., Ridley, D., McConnell, J., Sharma, S. et al.: 1980–2010 changes in Arctic Radiative Forcing from Aerosols, in preparation, 2015.

Browse, J., Carslaw, K. S., Arnold, S. R., Pringle, K., and Boucher, O.: The scavenging processes controlling the seasonal cycle in Arctic sulphate and black carbon aerosol, Atmos. Chem. Phys., 12, 6775–6798, doi:10.5194/acp-12-6775-2012, 2012.

ACPD

15, 29079–29124, 2015

Browse, J., Carslaw, K. S., Mann, G. W., Birch, C. E., Arnold, S. R., and Leck, C.: The complex response of Arctic aerosol to sea-ice retreat, Atmos. Chem. Phys., 14, 7543–7557, doi:10.5194/acp-14-7543-2014, 2014.

Cesana, G., Kay, J. E., Chepfer, H., English, J. M., and de Boer, G.: Ubiquitous low-level liquid-containing Arctic clouds: new observations and climate model constraints from CALIPSO-GOCCP, Geophys. Res. Lett., 39, L20804, doi:10.1029/2012GL053385, 2012.

Charlson, R. J., Schwartz, S. E., Hales, J. M., Cess, R. D., Coakley, J. A., Hansen, J. E., and Hofman, D. J.: Climate forcing by anthropogenic aerosols, Science, 255, 423–430, 1992.

Croft, B., Wentworth, G., Leaitch, W. R., Kodros, J., Murphy, J. G., Abbatt, J. P. D., Martin, R. V., and Pierce, J. R.: Arctic seabird emissions contribute to new-particle formation and radiative effects, in preparation, 2015.

D'Andrea, S. D., Häkkinen, S. A. K., Westervelt, D. M., Kuang, C., Levin, E. J. T., Kanawade, V. P., Leaitch, W. R., Spracklen, D. V., Riipinen, I., and Pierce, J. R.: Understanding global secondary organic aerosol amount and size-resolved condensational behavior, Atmos. Chem. Phys., 13, 11519–11534, doi:10.5194/acp-13-11519-2013, 2013.

Di Pierro, M., Jaeglé, L., Eloranta, E. W., and Sharma, S.: Spatial and seasonal distribution of Arctic aerosols observed by the CALIOP satellite instrument (2006–2012), Atmos. Chem. Phys., 13, 7075–7095, doi:10.5194/acp-13-7075-2013, 2013.

Engvall, A. C., Krejci, R., Ström, J., Minikin, A., Treffeisen, R., Stohl, A., and Herber, A.: In-situ airborne observations of the microphysical properties of the Arctic tropospheric aerosol during late spring and summer, Tellus B, 60, 392–404, doi:10.1111/j.1600-0889.2008.00348.x, 2008.

Fu, P. Q., Kawamura, K., Chen, J., Charrière, B., and Sempéré, R.: Organic molecular composition of marine aerosols over the Arctic Ocean in summer: contributions of primary emission and secondary aerosol formation, Biogeosciences, 10, 653–667, doi:10.5194/bg-10-653-2013, 2013.

Garrett, T. J., Zhao, C., and Novelli, P. C.: Assessing the relative contributions of transport efficiency and scavenging to seasonal variability in Arctic aerosol, Tellus B, 62, 190–196, doi:10.1111/j.1600-0889.2010.00453.x, 2010.

Garrett, T. J., Brattström, S., Sharma, S., Worthy, D. E. J., and Novelli, P.: The role of scavenging in the seasonal transport of black carbon and sulfate to the Arctic, Geophys. Res. Lett., 38, L16805, doi:10.1029/2011GL048221, 2011.

ACPD
15, 29079–29124, 2015

Ghan, S. J., Rissman, T. A., Elleman, R., Ferrare, R. A., Turner, D., Flynn, C., Wang, J., Ogren, J., Hudson, J., Jonsson, H. H., VanReken, T., Flagan, R. C., and Seinfeld, J. H.: Use of in situ cloud condensation nuclei, extinction, and aerosol size distribution measurements to test a method for retrieving cloud condensation nuclei profiles from surface measurements, J. Geophys. Res., 111, D05S10, doi:10.1029/2004JD005752, 2006.

Giorgi, F. and Chameides, W. L.: Rainout lifetimes of highly soluble aerosols and gases as inferred from simulations with a general circulation model, J. Geophys. Res., 91, 14367–14376, 1986.

Haywood, J. M. and Boucher, O.: Estimates of the direct and indirect radiative forcing due to tropospheric aerosols: a review, Rev. Geophys., 38, 513–543, 2000.

Heintzenberg, J., Leck, C., and Tunved, P.: Potential source regions and processes of aerosol in the summer Arctic, Atmos. Chem. Phys., 15, 6487–6502, doi:10.5194/acp-15-6487-2015, 2015.

Herzog, M., Weisenstein, D. K., and Penner, J. E.: A dynamic aerosol module for global chemical transport models: model description, J. Geophys. Res.-Atmos., 109, D18202, doi:10.1029/2003JD004405, 2004.

Hoose, C., Lohmann, U., Bennartz, R., Croft, B., and Lesins, G.: Global simulations of aerosol processing in clouds, Atmos. Chem. Phys. Discuss., 8, 13555–13618, doi:10.5194/acpd-8-13555-2008, 2008.

Kerminen, V. M., Anttila, T., Lehtinen, K. E. J., and Kulmala, M.: Parameterization for atmospheric new-particle formation: application to a system involving sulfuric acid and condensable water-soluble organic vapors, Aerosol Sci. Tech., 38, 1001–1008, 2004.

Korhonen, H., Carslaw, K. S., Spracklen, D. V., Ridley, D. A., and Ström, J.: A global model study of processes controlling aerosol size distributions in the Arctic spring and summer, J. Geophys. Res., 113, 1–20, doi:10.1029/2007JD009114, 2008.

Kristiansen, N. I., Stohl, A., Olivié, D. J. L., Croft, B., Søvde, O. A., Klein, H., Christoudias, T., Kunkel, D., Leadbetter, S. J., Lee, Y. H., Zhang, K., Tsigaridis, K., Bergman, T., Evangeliou, N., Wang, H., Ma, P.-L., Easter, R. C., Rasch, P. J., Liu, X., Pitari, G., Di Genova, G., Zhao, S. Y., Balkanski, Y., Bauer, S. E., Faluvegi, G. S., Kokkola, H., Martin, R. V., Pierce, J. R., Schulz, M., Shindell, D., Tost, H., and Zhang, H.: Evaluation of observed and modelled aerosol lifetimes using radioactive tracers of opportunity and an ensemble of 19 global models, Atmos. Chem. Phys. Discuss., 15, 24513–24585, doi:10.5194/acpd-15-24513-2015, 2015.

ACPD
15, 29079–29124, 2015

Leaitch, W. R., Sharma, S., Huang, L., Toom-Sauntry, D., Chivulescu, A., Macdonald, A. M., von Salzen, K., Pierce, J. R., Bertram, A. K., Schroder, J. C., Shantz, N. C., Chang, R. Y. W., and Norman, A.-L.: Dimethyl sulfide control of the clean summertime Arctic aerosol and cloud, Elementa, 1, 17, doi:10.12952/journal.elementa.000017, 2013.

Leaitch, W. R., Korolev, A., Aliabadi, A., Burkhart, J., Willis, M., Abbatt, J. P. D., Bozem, H., Hoor, P., Köllner, F., Schneider, J., Herber, A., Konrad, J., and Brauner, R.: Observations of aerosol and liquid-cloud microphysics in the Canadian Arctic during summer, J. Geophys. Res., under review, 2015.

Lee, L. A., Pringle, K. J., Reddington, C. L., Mann, G. W., Stier, P., Spracklen, D. V., Pierce, J. R., and Carslaw, K. S.: The magnitude and causes of uncertainty in global model simulations of cloud condensation nuclei, Atmos. Chem. Phys., 13, 8879–8914, doi:10.5194/acp-13-8879-2013, 2013.

Lee, Y. H. and Adams, P. J.: A fast and efficient version of the TwO-Moment Aerosol Sectional (TOMAS) global aerosol microphysics model, Aerosol Sci. Tech., 46, 678–689, doi:10.1080/02786826.2011.643259, 2012.

Lee, Y. H., Pierce, J. R., and Adams, P. J.: Representation of nucleation mode microphysics in a global aerosol model with sectional microphysics, Geosci. Model Dev., 6, 1221–1232, doi:10.5194/gmd-6-1221-2013, 2013.

Liu, H., Jacob, D. J., Bey, I., and Yantosca, R. M.: Constraints from ^{210}Pb and ^{7}Be on wet deposition and transport in a global three-dimensional chemical tracer model driven by assimilated meteorological fields, J. Geophys. Res., 106, 12109–12128, 2001.

Lohmann, U. and Feichter, J.: Global indirect aerosol effects: a review, Atmos. Chem. Phys. Discuss., 4, 7561–7614, doi:10.5194/acpd-4-7561-2004, 2004.

Mann, G. W., Carslaw, K. S., Spracklen, D. V., Ridley, D. A., Manktelow, P. T., Chipperfield, M. P., Pickering, S. J., and Johnson, C. E.: Description and evaluation of GLOMAP-mode: a modal global aerosol microphysics model for the UKCA composition-climate model, Geosci. Model Dev. Discuss., 3, 651–734, doi:10.5194/gmdd-3-651-2010, 2010.

Mann, G. W., Carslaw, K. S., Ridley, D. A., Spracklen, D. V., Pringle, K. J., Merikanto, J., Korhonen, H., Schwarz, J. P., Lee, L. A., Manktelow, P. T., Woodhouse, M. T., Schmidt, A., Breider, T. J., Emmerson, K. M., Reddington, C. L., Chipperfield, M. P., and Pickering, S. J.: Intercomparison of modal and sectional aerosol microphysics representations within the same 3-D global chemical transport model, Atmos. Chem. Phys., 12, 4449–4476, doi:10.5194/acp-12-4449-2012, 2012.

ACPD
15, 29079–29124, 2015

Napari, I., Noppel, M., Vehkamaki, H., and Kulmala, M.: Parametrization of ternary nucleation rates for H_2SO_4-NH_3-H_2O vapors, J. Geophys. Res., 107, 4310–4381, 2002.
O'Dowd, C. D. and de Leeuw, G.: Marine aerosol production: a review of the current knowledge, Philos. T. R. Soc. A , 365, 1753–1774, doi:10.1098/rsta.2007.2043, 2007.
Olenius, T., Kupiainen-Määttä, O., Ortega, I. K., Kurtén, T., and Vehkamäki, H.: Free energy barrier in the growth of sulfuric acid-ammonia and sulfuric acid-dimethylamine clusters, J. Chem. Phys., 139, 084312, doi:10.1063/1.4819024, 2013.
Pierce, J. R. and Adams, P. J.: Uncertainty in global CCN concentrations from uncertain aerosol nucleation and primary emission rates, Atmos. Chem. Phys., 9, 1339–1356, doi:10.5194/acp-9-1339-2009, 2009.
Pierce, J. R., Evans, M. J., Scott, C. E., D'Andrea, S. D., Farmer, D. K., Swietlicki, E., and Spracklen, D. V.: Weak global sensitivity of cloud condensation nuclei and the aerosol indirect effect to Criegee + SO_2 chemistry, Atmos. Chem. Phys., 13, 3163–3176, doi:10.5194/acp-13-3163-2013, 2013.
Pierce, J. R., Croft, B., Kodros, J. K., D'Andrea, S. D., and Martin, R. V.: The importance of interstitial particle scavenging by cloud droplets in shaping the remote aerosol size distribution and global aerosol-climate effects, Atmos. Chem. Phys., 15, 6147–6158, doi:10.5194/acp-15-6147-2015, 2015.
Riddick, S. N., Dragosits, U., Blackall, T. D., Daunt, F., Wanless, S., and Sutton, M. A.: The global distribution of ammonia emissions from seabird colonies, Atmos. Environ., 55, 319–327, doi:10.1016/j.atmosenv.2012.02.052, 2012.
Seabird Information Network: Circumpolar Seabird Data Portal, available at: http://axiom.seabirds.net/circumpolar_portal.php (last access: 13 March 2015), 2015.
Sharma, S., Ishizawa, M., Chan, D., Lavoué, D., Andrews, E., Eleftheriadis, K., and Maksyutov, S.: 16-year simulation of Arctic black carbon: transport, source contribution, and sensitivity analysis on deposition, J. Geophys. Res.-Atmos., 118, 943–964, doi:10.1029/2012JD017774, 2013.
Shupe, M. D., Uttal, T., Matrosov, S. Y., and Frisch, A. S.: Cloud water contents and hydrometeor sizes during the FIRE Arctic clouds experiment, J. Geophys. Res., 106, 15015–15028, 2001.
Spracklen, D. V., Pringle, K. J., Carslaw, K. S., Chipperfield, M. P., and Mann, G. W.: A global off-line model of size-resolved aerosol microphysics: I. Model development and prediction of aerosol properties, Atmos. Chem. Phys., 5, 2227–2252, doi:10.5194/acp-5-2227-2005, 2005a.

ACPD
15, 29079–29124, 2015

Spracklen, D. V., Pringle, K. J., Carslaw, K. S., Chipperfield, M. P., and Mann, G. W.: A global off-line model of size-resolved aerosol microphysics: II. Identification of key uncertainties, Atmos. Chem. Phys., 5, 3233–3250, doi:10.5194/acp-5-3233-2005, 2005b.

Spracklen, D. V, Carslaw, K. S., Kulmala, M., Kerminen, V. M., Sihto, S. L., Riipinen, I., Merikanto, J., Mann, G. W., Chipperfield, M. P., Wiedensohler, A., Birmili, W., and Lihavainen, H.: Contribution of particle formation to global cloud condensation nuclei concentrations, Geophys. Res. Lett., 35, D06808, doi:10.1029/2007GL033038, 2008.

Stevens, R. G. and Pierce, J. R.: The contribution of plume-scale nucleation to global and regional aerosol and CCN concentrations: evaluation and sensitivity to emissions changes, Atmos. Chem. Phys. Discuss., 14, 21473–21521, doi:10.5194/acpd-14-21473-2014, 2014.

Stohl, A., Klimont, Z., Eckhardt, S., Kupiainen, K., Shevchenko, V. P., Kopeikin, V. M., and Novigatsky, A. N.: Black carbon in the Arctic: the underestimated role of gas flaring and residential combustion emissions, Atmos. Chem. Phys., 13, 8833–8855, doi:10.5194/acp-13-8833-2013, 2013.

Trivitayanurak, W., Adams, P. J., Spracklen, D. V., and Carslaw, K. S.: Tropospheric aerosol microphysics simulation with assimilated meteorology: model description and intermodel comparison, Atmos. Chem. Phys., 8, 3149–3168, doi:10.5194/acp-8-3149-2008, 2008.

Tunved, P., Ström, J., and Hansson, H.-C.: An investigation of processes controlling the evolution of the boundary layer aerosol size distribution properties at the Swedish background station Aspvreten, Atmos. Chem. Phys. Discuss., 4, 4507–4543, doi:10.5194/acpd-4-4507-2004, 2004.

Tunved, P., Ström, J., and Krejci, R.: Arctic aerosol life cycle: linking aerosol size distributions observed between 2000 and 2010 with air mass transport and precipitation at Zeppelin station, Ny-Ålesund, Svalbard, Atmos. Chem. Phys., 13, 3643–3660, doi:10.5194/acp-13-3643-2013, 2013.

Twomey, S.: Pollution and the planetary albedo, Atmos. Environ., 8, 1251–1256, 1974.

Vehkamäki, H., Kulmala, M., Napari, I., Lehtinen, K. E. J., Timmreck, C., Noppel, M., and Laaksonen, A.: An improved parameterization for sulfuric acid-water nucleation rates for tropospheric and stratospheric conditions, J. Geophys. Res., 107, 4610–4622, 2002.

Verheggen, B., Cozic, J., Weingartner, E., Bower, K., Mertes, S., Connolly, P., Gallagher, M., Flynn, M., Choularton, T., and Baltensperger, U.: Aerosol partitioning between the interstitial and the condensed phase in mixed-phase clouds, J. Geophys. Res., 112, D23202, doi:10.1029/2007JD008714, 2007.

ACPD
15, 29079–29124, 2015

Wang, M. and Penner, J. E.: Aerosol indirect forcing in a global model with particle nucleation, Atmos. Chem. Phys., 9, 239–260, doi:10.5194/acp-9-239-2009, 2009.

Wang, Q., Jacob, D. J., Fisher, J. A., Mao, J., Leibensperger, E. M., Carouge, C. C., Le Sager, P., Kondo, Y., Jimenez, J. L., Cubison, M. J., and Doherty, S. J.: Sources of carbonaceous aerosols and deposited black carbon in the Arctic in winter-spring: implications for radiative forcing, Atmos. Chem. Phys., 11, 12453–12473, doi:10.5194/acp-11-12453-2011, 2011.

Wentworth, G. R., Murphy, J. G., Croft, B., Martin, R. V., Pierce, J. R., Cote, J.-S., Courchesne, I., Tremblay, J.-E., Gagnon, J., Thomas, J. L., Sharma, S., Toom-Sauntry, D., Chivulescu, A., Levasseur, M., and Abbatt, J. P. D.: Ammonia in the summertime Arctic marine boundary layer: sources, sinks and implications, Atmos. Chem. Phys. Discuss., in press, 2015.

Westervelt, D. M., Pierce, J. R., Riipinen, I., Trivitayanurak, W., Hamed, A., Kulmala, M., Laaksonen, A., Decesari, S., and Adams, P. J.: Formation and growth of nucleated particles into cloud condensation nuclei: model–measurement comparison, Atmos. Chem. Phys., 13, 7645–7663, doi:10.5194/acp-13-7645-2013, 2013.

Williams, J., de Reus, M., Krejci, R., Fischer, H., and Ström, J.: Application of the variability–size relationship to atmospheric aerosol studies: estimating aerosol lifetimes and ages, Atmos. Chem. Phys., 2, 43–74, doi:10.5194/acpd-2-43-2002, 2002.

Yu, F.: A secondary organic aerosol formation model considering successive oxidation aging and kinetic condensation of organic compounds: global scale implications, Atmos. Chem. Phys., 11, 1083–1099, doi:10.5194/acp-11-1083-2011, 2011.

Yu, F. and Luo, G.: Simulation of particle size distribution with a global aerosol model: contribution of nucleation to aerosol and CCN number concentrations, Atmos. Chem. Phys., 9, 7691–7710, doi:10.5194/acp-9-7691-2009, 2009.

ACPD
15, 29079–29124, 2015

Table 1. Summary of the simulations conducted for this study.

Simulation Name	Revised Wet Removal	With Interstitial Coagulation	With New Particle Formation
STD	no	no	yes
NEWSCAV	yes	no	yes
NEWSCAV + COAG	yes	yes	yes
NONUC	yes	no	no

ACPD
15, 29079–29124, 2015

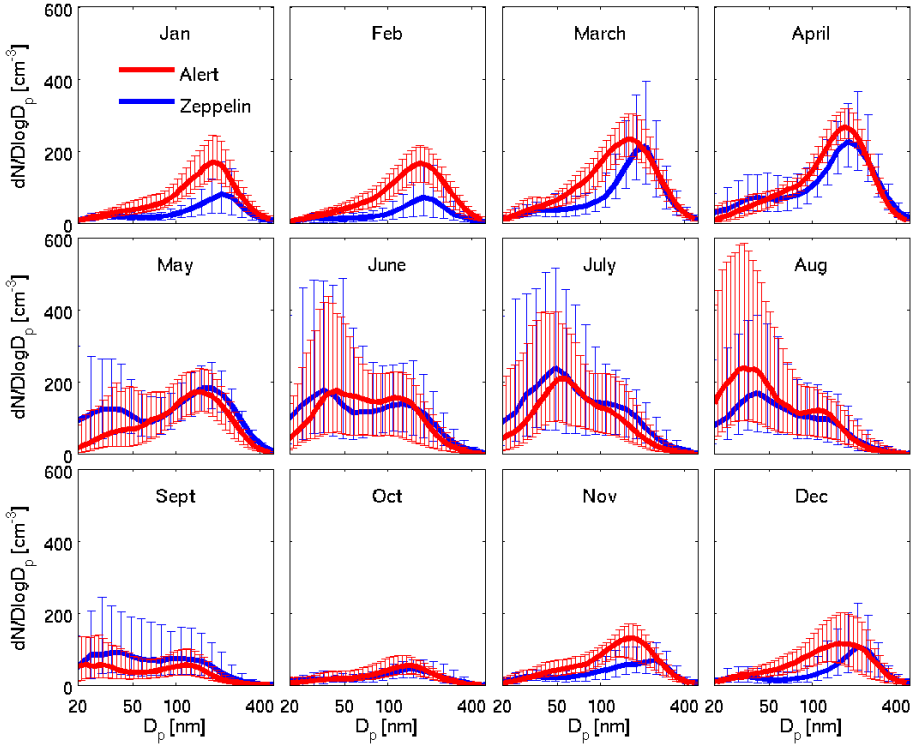

Figure 1. Measured monthly median number distributions from the scanning mobility particle sizer (SMPS) at Alert for 2011–2013 and the differential mobility particle sizer (DMPS) at Mt. Zeppelin for 2011–2013 for particle sizes between 20 and 500 nm. Error bars show the 20–80th percentile of the measurements.

ACPD
15, 29079–29124, 2015

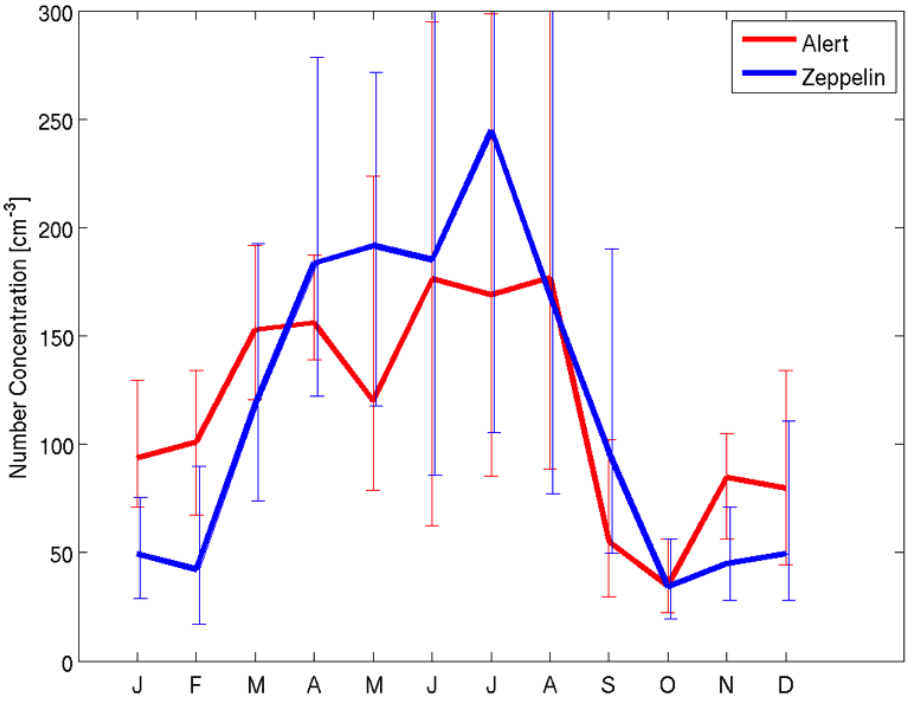

Figure 2. Measurement monthly median integrated aerosol number concentrations [cm^{-3}] at standard temperature and pressure from SMPS at Alert (2011–2013), and DMPS at Mt. Zeppelin (2011–2013) for particle sizes between 20 and 500 nm. Error bars show the 20th and 80th percentiles.

ACPD
15, 29079–29124, 2015

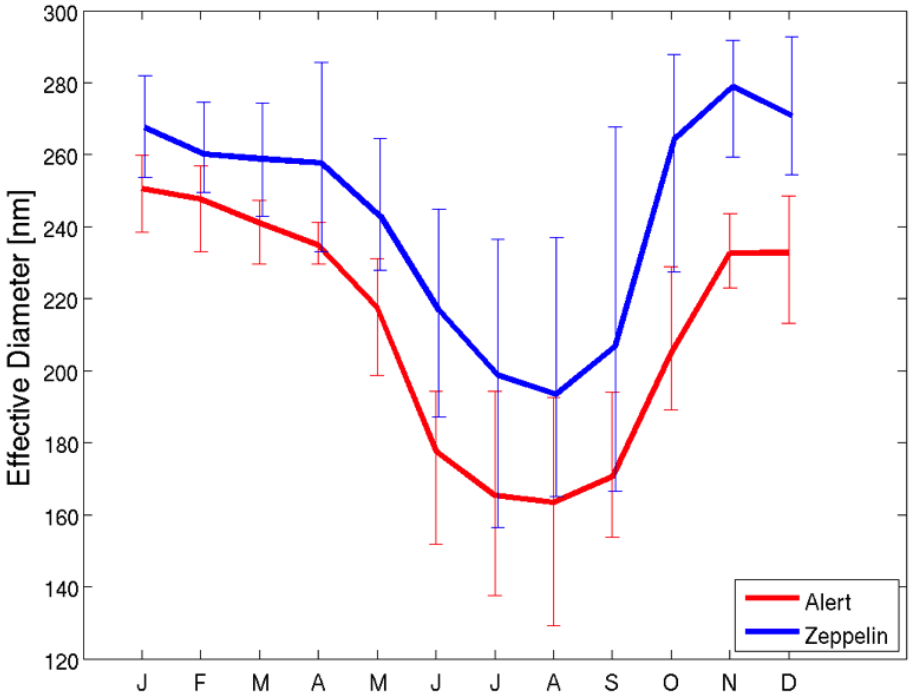

Figure 3. Measurement monthly median aerosol effective diameter from SMPS and DMPS at the two high-Arctic sites, Alert (2011–2013) and Mt. Zeppelin (2011–2013), respectively, for particle sizes between 20 and 500 nm. Error bars show the 20th and 80th percentiles.

ACPD
15, 29079–29124, 2015

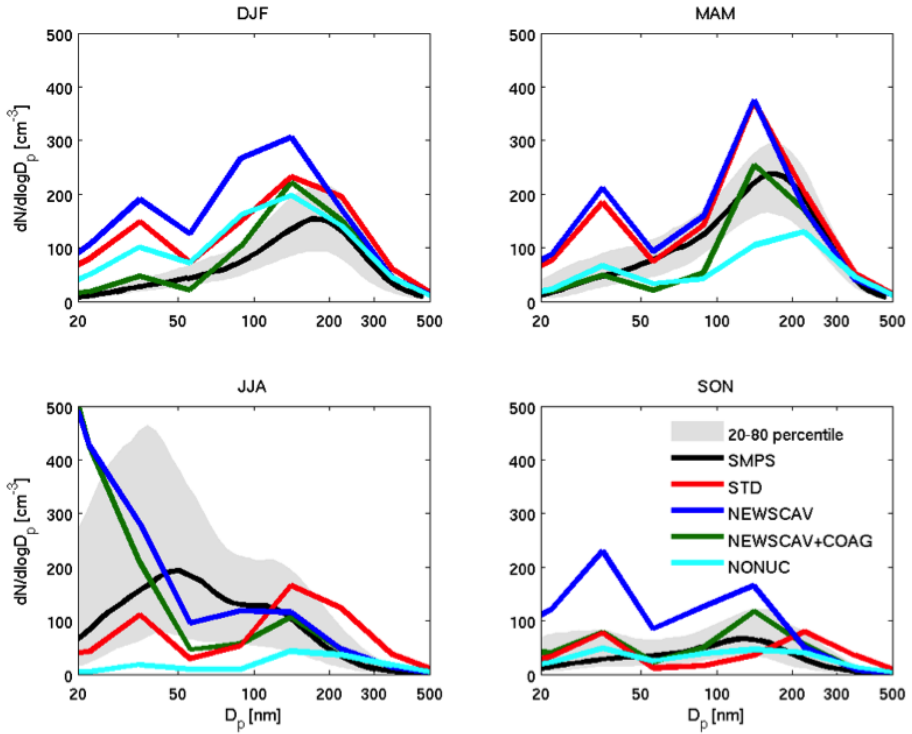

Figure 4. Seasonal median number distributions from SMPS measurements at Alert (2011–2013) and for the GEOS-Chem-TOMAS simulations (described in Table 1), with the measurement 20–80th percentile in grey shading. Simulations are shown in color as indicated by legend.

ACPD
15, 29079–29124, 2015

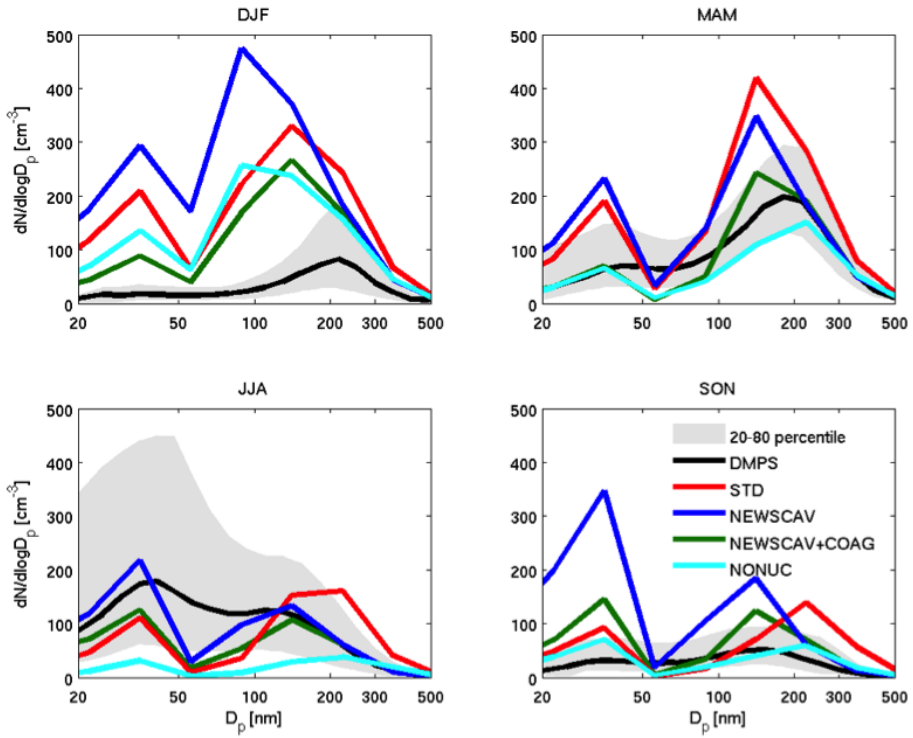

Figure 5. Seasonal median number distributions from DMPS measurements at Mt. Zeppelin (2011–2013) and for the GEOS-Chem-TOMAS simulations (described in Table 1), with the measurement 20–80th percentile in grey shading. Simulations are shown in color as indicated by legend.

ACPD
15, 29079–29124, 2015

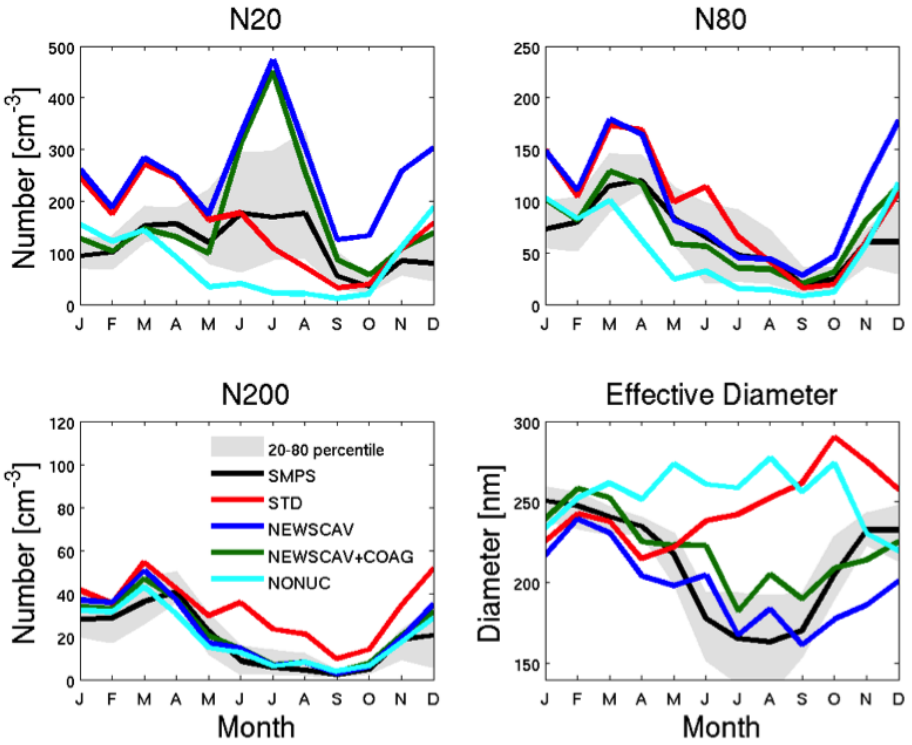

Figure 6. Monthly median number concentration for aerosols with diameters of 20–500 nm (N20), 80–500 nm (N80), and 200–500 nm (N200), and effective diameter from the 2011–2013 Alert SMPS measurements and for the four GEOS-Chem-TOMAS simulations described in Table 1. Simulations are shown in color as indicated by legend.

ACPD
15, 29079–29124, 2015

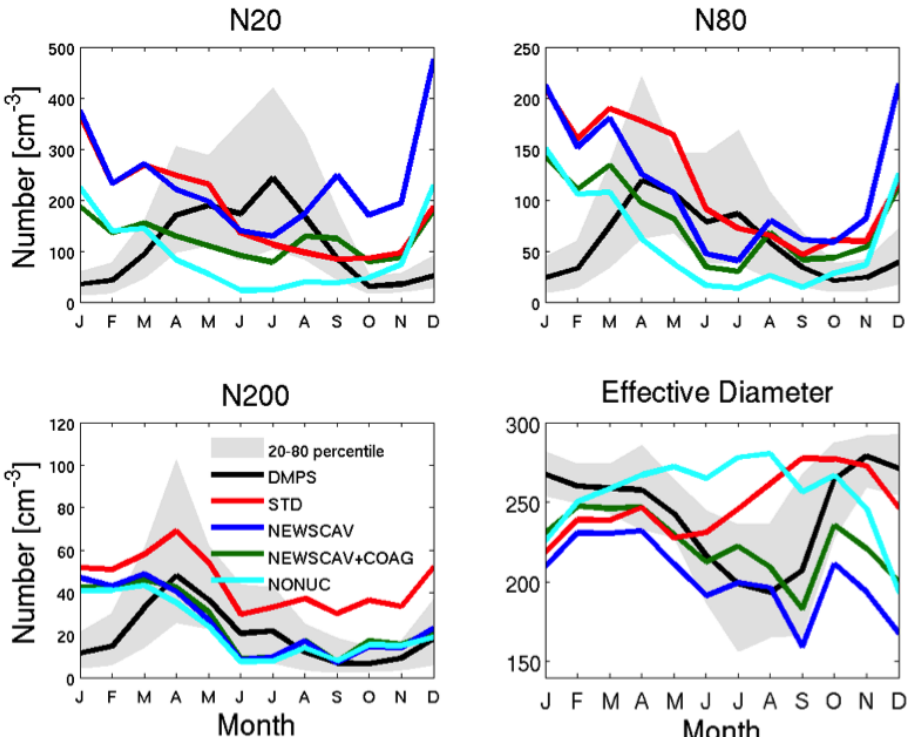

Figure 7. Monthly median number concentration for aerosols with diameters of 20–500 nm (N20), 80–500 nm (N80), and 200–500 nm (N200), and effective diameter from the 2011–2013 Mt. Zeppelin DMPS measurements and for the four GEOS-Chem-TOMAS simulations described in Table 1. Simulations are shown in color as indicated by legend.

ACPD
15, 29079–29124, 2015

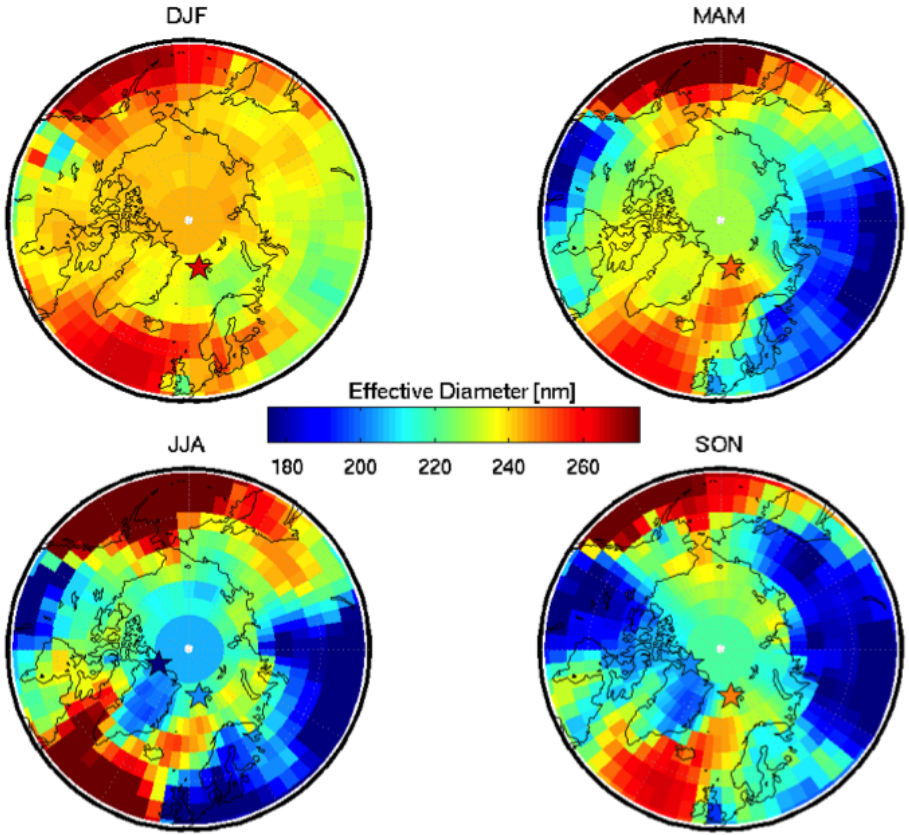

Figure 8. Geographic distribution of the simulated pan-Arctic surface-layer seasonal-mean dry effective diameter [nm] for the NEWSCAV + COAG simulation. The colored stars indicate the effective diameter from measurements at Alert (SMPS) and Mt. Zeppelin (DMPS).

ACPD
15, 29079–29124, 2015

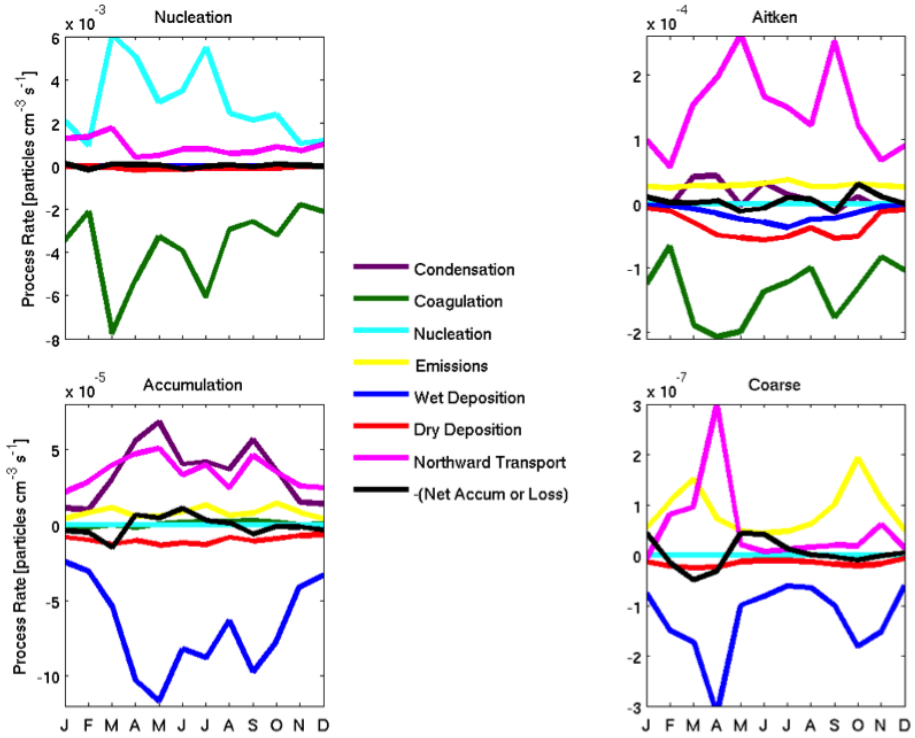

Figure 9. Monthly and Arctic mean aerosol number process rates for the entire Arctic troposphere (north of 66° N) for simulation NEWSCAV + COAG. Processes considered for each of four size ranges are nucleation, emissions, coagulation, condensation, wet and dry deposition, transport across 66° N and net regional accumulation or loss rates. The aerosol size ranges are nucleation (D_p < 10 nm), Aitken (10 < D_p < 100 nm), accumulation (100 < D_p < 1000 nm), and coarse (D_p > 1000 nm).

ACPD
15, 29079–29124, 2015

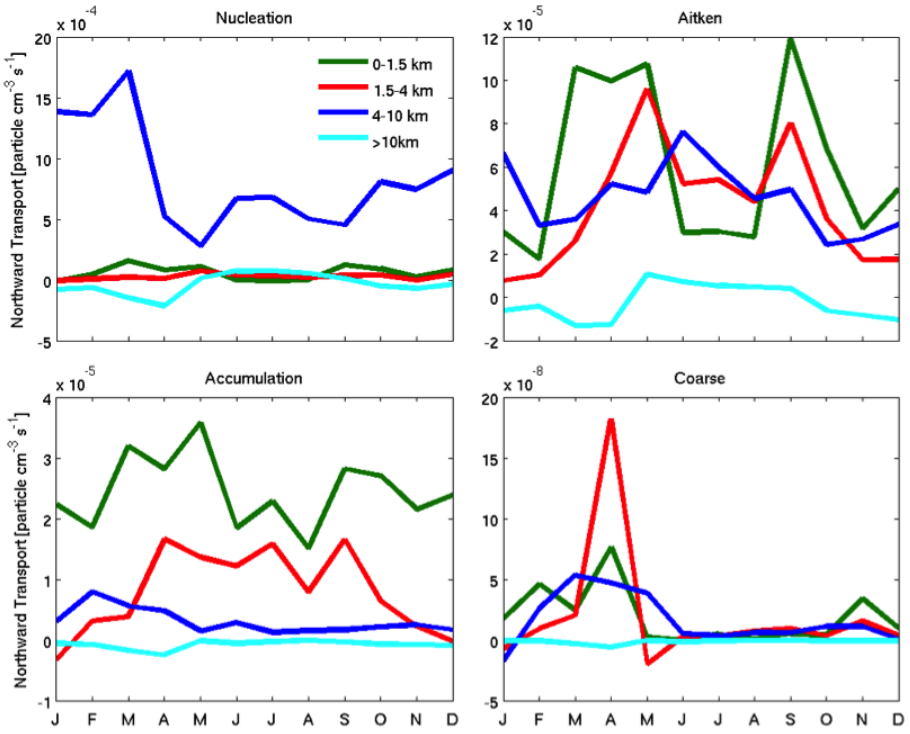

Figure 10. Monthly and Arctic mean aerosol number tendency due to transport within each of four vertical layers between (1) 0–1.5 km, (2) 1.5–4 km, (3) 4–10 km, and (4) above 10 km for the simulation NEWSCAV + COAG as this contributes to aerosol number considering the entire troposphere north of 66° N and for the four aerosol size ranges: nucleation, Aitken, accumulation, and coarse described in Fig. 9. Summation of the 4 tendencies for any given month and size range yields the transport tendency shown in Fig. 9. Positive values indicate a net northward transport into the Arctic.

ACPD
15, 29079–29124, 2015

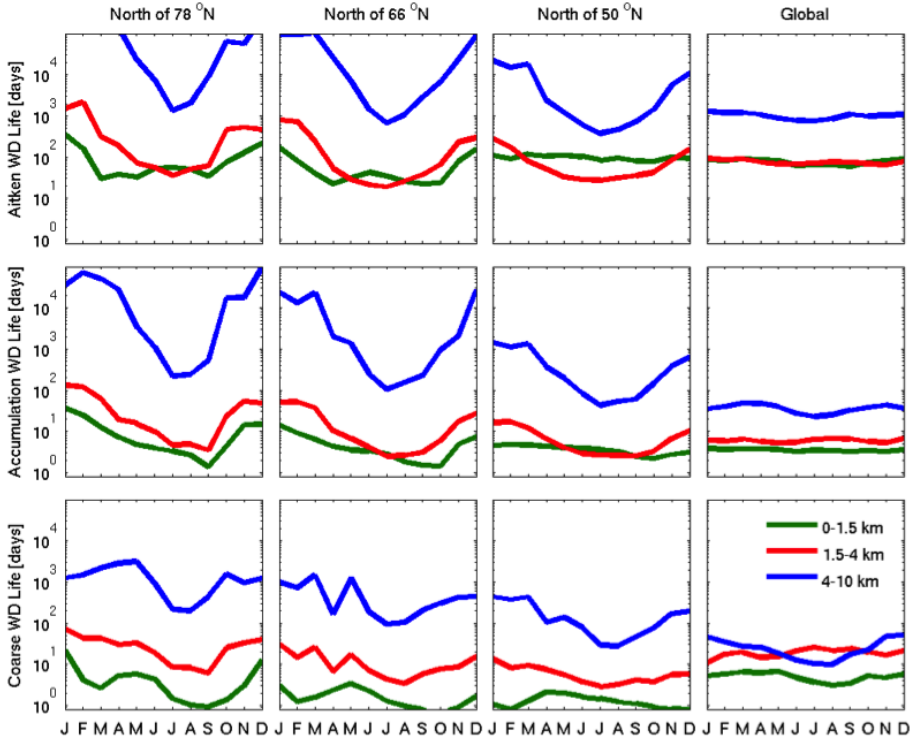

Figure 11. Regional and monthly mean aerosol number lifetime with respect to wet deposition for the aerosol size ranges: Aitken ($10 < D_p < 100$ nm), accumulation ($100 < D_p < 1000$ nm), and coarse ($D_p > 1000$ nm), for four regions, and in the altitude bands of 0–1.5, 1.5–4, and 4–10 km for the GEOS-Chem simulation NEWSCAV + COAG.

ACPD
15, 29079–29124, 2015

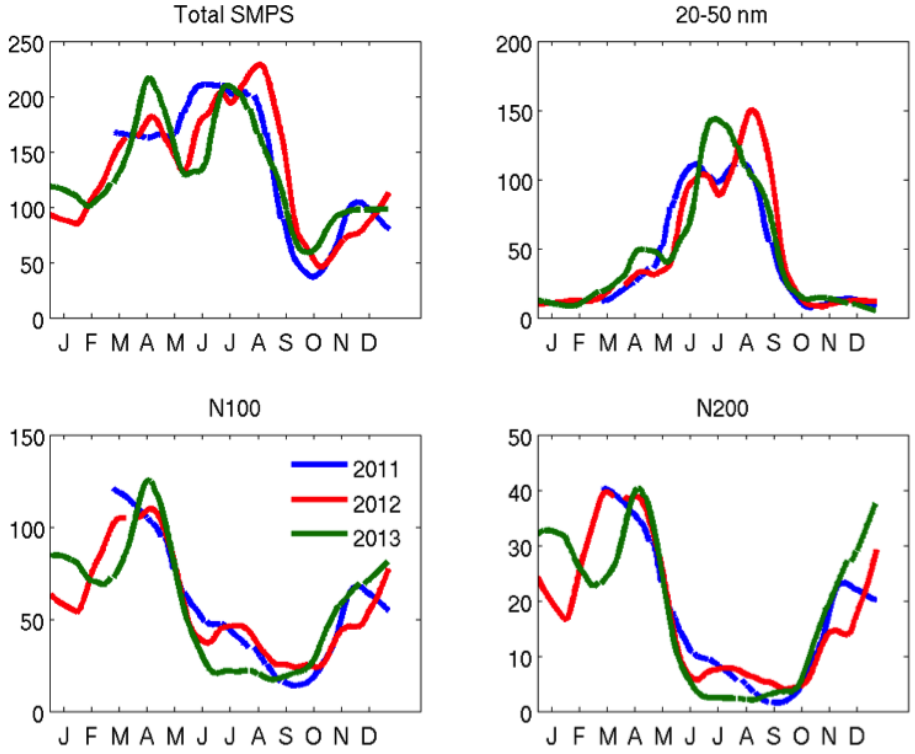

Figure A1. Seasonal cycle of total SMPS particle number (particle diameters 20–500 nm), particle number with diameters 20–50 nm, particle number with diameters 100–500 nm (N100), and particle number with diameters 200–500 nm (N200) from SMPS at Alert for 2011, 2012 and 2013. Values are 4-week running mean.

ACPD
15, 29079–29124, 2015

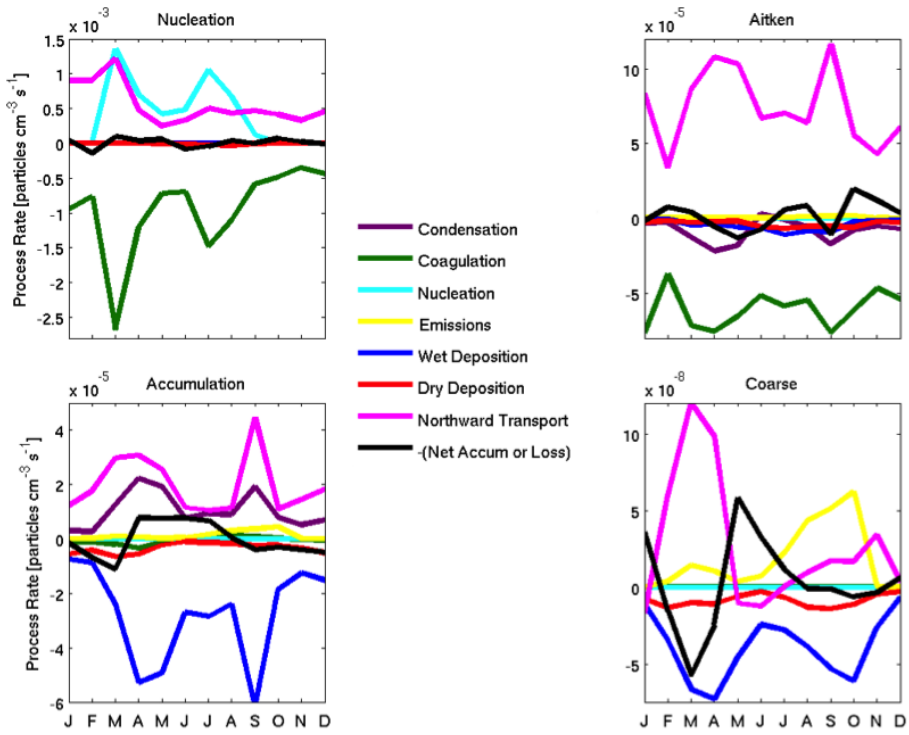

Figure A2. Regional and monthly mean aerosol number process rates for entire troposphere north of 78° N for the simulation NEWSCAV + COAG. The four aerosol size ranges are described in Fig. 9.

ACPD
15, 29079–29124, 2015

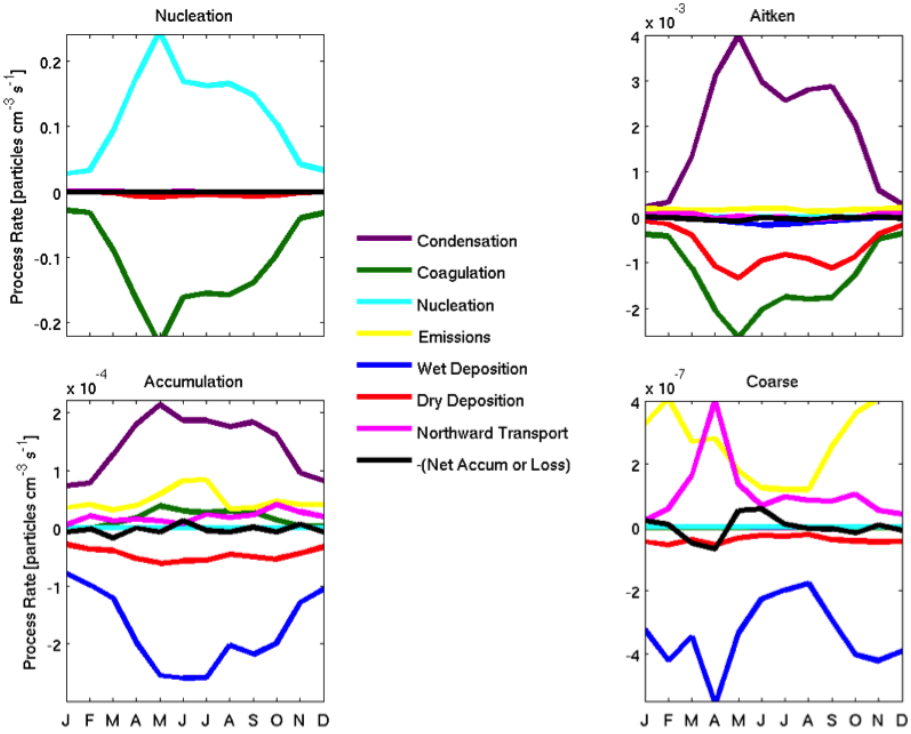

Figure A3. Regional and monthly mean aerosol number process rates for entire troposphere of north of 50° N for the simulation NEWSCAV + COAG. The four aerosol size ranges are described in Fig. 9.

ACPD
15, 29079–29124, 2015

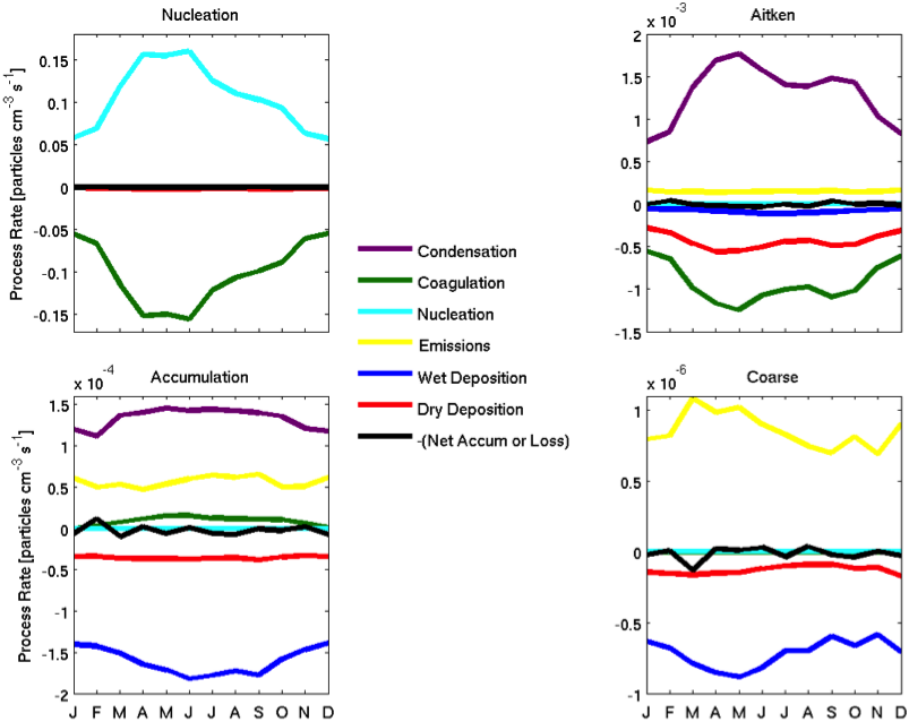

Figure A4. Global and monthly mean aerosol number process rates for entire troposphere for the simulation NEWSCAV + COAG. The four aerosol size ranges are described in Fig. 9.

ACPD
15, 29079–29124, 2015